

Chiral and nodal superconductors in t-J model with valley contrasting flux on triangular moiré lattice

Boran Zhou and Ya-Hui Zhang

Department of Physics and Astronomy, Johns Hopkins University, Baltimore, Maryland 21218, USA

Recent experimental progresses have made it possible to simulate spin 1/2 Hubbard model on triangular lattice in moiré materials formed by transition metal dichalcogenide (TMD) heterobilayer or homobilayer. In twisted TMD homobilayer, a vertical electric field can induce a valley contrasting flux in the hopping term. In this paper we study possible superconductors from a t-J model with valley contrasting flux Φ using the slave boson mean field theory. We obtain a phase diagram with doping x and Φ . A finite Φ breaks spin rotation symmetry and the pairing symmetry is a superposition of spin singlet $d - id$ and spin triplet $p + ip$. There are two topological phase transitions when tuning Φ from 0 to π , with three Dirac nodes at one transition and one single Dirac node at the other transition. We also discuss the effects of van Hove singularity and a three-site correlated hopping term on the pairing strength. Lastly, we demonstrate that a small anisotropy term breaking the C_3 rotation can lead to a time reversal invariant nodal superconductor connected to the $d_{x^2-y^2}$ superconductor on square lattice.

Introduction– Superconductivity from doping a Mott insulator has been intensively studied in the last several decades after the discovery of the high T_c superconductor in cuprates[1]. Recently, moiré superlattices emerge to be a wonderful platform to simulate strongly correlated physics[2–22]. Superconductivity has been experimentally reported in twisted bilayer graphene and twisted multilayer graphene system with alternating twist angles[5, 23–25]. However, mechanism of the superconductivity there is still under debate. Theoretical study in TBG is hard due to the lack of a simple lattice model which is obstructed by the fragile topology[26]. On the other hand, moiré superlattice based on transition metal dichalcogenide (TMD) is believed to be described by a simple Hubbard model[27] similar to that of the cuprate. This offers an opportunity to study superconductivity in Hubbard model or t-J model on triangular lattice.

Moiré superlattice can be formed by twisting TMD homo-bilayer or hetero-bilayer. In both cases the resulting Hubbard model has two flavors from the two valley, which are locked to the spins due to the strong Ising spin-orbit coupling of the valence band. In the hetero-bilayer case, it was shown that there is a good SU(2) spin rotation symmetry in the valley (spin) space[27]. Thus the physics of doping the Mott insulator at $\nu_T = 1$ is captured by the standard t-J model. In contrast, for the twisting TMD homo-bilayer [28], the low energy model has a valley contrasting flux Φ induced by a displacement field in the z direction[29, 30]. The valley contrasting flux origins from the inversion symmetry breaking within each valley and is known to exist also in graphene moiré systems[31]. In such a case, the SU(2) spin rotation symmetry is broken down to U(1) except at $\Phi = 0 \bmod 2\pi$. The t-J model with $\Phi = 0$ has been found to host a $d - id$ superconductor by the slave boson mean field theory[32]. But the fate at generic Φ is unknown, although there are already a few studies at weak coupling limit [33–35]. For application to twisted TMD homobilayer, it is desirable

to obtain a phase diagram of (n, Φ) given that both the density n and Φ can be conveniently tuned in the dual gated sample.

In this paper we perform a slave boson mean field study of the t-J model with a generic valley contrasting flux Φ . The flux Φ enters both the hopping term and the J term through a Dzyaloshinskii-Moriya (DM) interaction. At finite Φ , we find that the $d - id$ spin-singlet pairing is mixed with a $p + ip$ spin-triplet pairing. By changing Φ at fixed density n , we find two topological phase transitions between Chern number $|C| = 2$ and $|C| = 1$ through three Dirac nodes and one Dirac node respectively. We also notice the correlations between the density of states (DOS) and the pairing strength. Pairing is stronger at the van hove singularity. Chiral superconductivity has been observed in numerical simulations in the SU(2) symmetric limit[36–38], our study demonstrates a new route to tune a topological phase transition through changing the valley contrasting flux. We also study the effect of strain which breaks the C_3 rotation symmetry. We find that a small strain favors a nodal superconductor with the same symmetry as the $d_{x^2-y^2}$ pairing in cuprates. This suggests that a nematic nodal superconductor is a strong competing state. Indeed recent numerical simulation shows that adding a J_2 term can lead to a transition from the chiral superconductor to the nematic nodal superconductor[38].

Model– The twisted TMD homobilayer can be described by a generalized triangular-lattice Hubbard model [39]:

$$H = - \sum_{\langle ij \rangle, s} \left(t e^{i\phi_{ij}^s} c_{i,s}^\dagger c_{j,s} + \text{H.c.} \right) + U \sum_i n_{i\uparrow} n_{i\downarrow} - \mu \sum_i (n_{i\uparrow} + n_{i\downarrow}), \quad (1)$$

where $s = \uparrow, \downarrow$ labels the valley index which is locked to the spin. $\langle ij \rangle$ represents the nearest-neighbor (NN) bond. We have $\phi_{ij}^\uparrow = -\phi_{ij}^\downarrow$ due to the time reversal sym-

metry. As illustrated in Fig.1, $\phi_{ij}^\uparrow = \pm\phi$ depending on the direction of the bond. There is a valley contrasting flux $\Phi = 3\phi$ and $-\Phi$ in the two types of triangles for one valley. We label σ_a as Pauli matrices in the valley space. We have time reversal symmetry \mathcal{T} acting as $\sigma_x \mathcal{K}$, where \mathcal{K} is the complex conjugate. The mirror reflection operators \mathcal{M}_x and \mathcal{M}_y act as $c_s(x, y) \rightarrow c_s(x, -y)$ and $c_s(x, y) \rightarrow (\sigma_x)_{ss'} c_{s'}(-x, y)$ respectively. C_6 around site \mathbf{x} acts as: $c_s(\mathbf{x}) \rightarrow (\sigma_x)_{ss'} c_{s'}(C_6 \mathbf{x})$. Two basis vectors of the lattice are $\mathbf{a}_1 = (1, 0)$ and $\mathbf{a}_2 = (-\frac{1}{2}, \frac{\sqrt{3}}{2})$. The corresponding reciprocal basis vectors are $\mathbf{b}_1 = (2\pi, \frac{2\pi}{\sqrt{3}})$ and $\mathbf{b}_2 = (0, \frac{4\pi}{\sqrt{3}})$. ϕ and $\phi + \frac{2\pi}{3}$ are gauge equivalent upon a transformation: $c_s(\mathbf{x}) \rightarrow (e^{i\frac{\pi}{3} \cdot (\mathbf{b}_1 + \mathbf{b}_2) \cdot \sigma_z})_{ss'} c_{s'}(\mathbf{x})$. We can combine a particle hole transformation with the gauge transformation: $c_s(\mathbf{x}) \rightarrow (e^{i\frac{\pi}{6} \cdot (\mathbf{b}_1 + \mathbf{b}_2) \cdot \sigma_z} \sigma_x)_{ss'} c_{s'}^\dagger(\mathbf{x})$, which maps Φ to $\Phi + \pi$ and the density n to $2 - n$ [33].

In the strong coupling limit $t \ll U$ and filling factor $n < 1$, we can use the standard t/U expansion [40] to obtain a t-J model [39]:

$$\begin{aligned}
 H = & - \sum_{\langle ij \rangle, s} P \left(t e^{i\phi_{ij}^s} c_{i,s}^\dagger c_{j,s} + \text{H.c.} \right) P + J \sum_{\langle ij \rangle} \left[S_i^z S_j^z \right. \\
 & + \cos(2\phi_{ij}^\uparrow) \sum_{\alpha=x,y} S_i^\alpha S_j^\alpha + \sin(2\phi_{ij}^\uparrow) (S_i^x S_j^y - S_i^y S_j^x) \\
 & \left. - \frac{1}{4} n_i n_j \right] - \mu \sum_i (n_{i\uparrow} + n_{i\downarrow}),
 \end{aligned} \tag{2}$$

where $J = \frac{4t^2}{U}$ and P is the projection operator which forbids double occupancy. For $\phi \neq 0$, the system only has a U(1) spin rotation symmetry generated by σ_z . At $n = 1$, the ground state is an XY ferromagnetic phase for $|\phi| \in (\frac{\pi}{3}, \frac{2\pi}{3})$, 120° AF⁺ phase for $\phi \in (0, \frac{\pi}{3}) \cup (\pi, \frac{4\pi}{3})$ and 120° AF⁻ phase for $\phi \in (\frac{2\pi}{3}, \pi) \cup (\frac{5\pi}{3}, 2\pi)$ [39]. The ground state remains unexplored at finite doping with $n = 1 - x$. We expect that the magnetic order is suppressed by the doping [32]. The major focus of this paper is to explore the possibility of superconducting phase in the small doping regimes. For the $n > 1$ case, we can apply the particle-hole transformation to map the model to the $n < 1$ model above, but with a change of the flux $\phi \rightarrow \phi + \pi$.

Slave boson mean field theory– Since it is difficult to handle the projection operator directly, we use the U(1) slave boson theory [1, 41] to deal with the model. We focus our discussion in the region $n < 1$, while the $n > 1$ regime can be obtained by the particle hole transformation. The electron operator can be represented as $c_{i,s}^\dagger = f_{i,s}^\dagger b_i$. By decoupling the interaction part in hopping and pairing channel, we use the following mean field

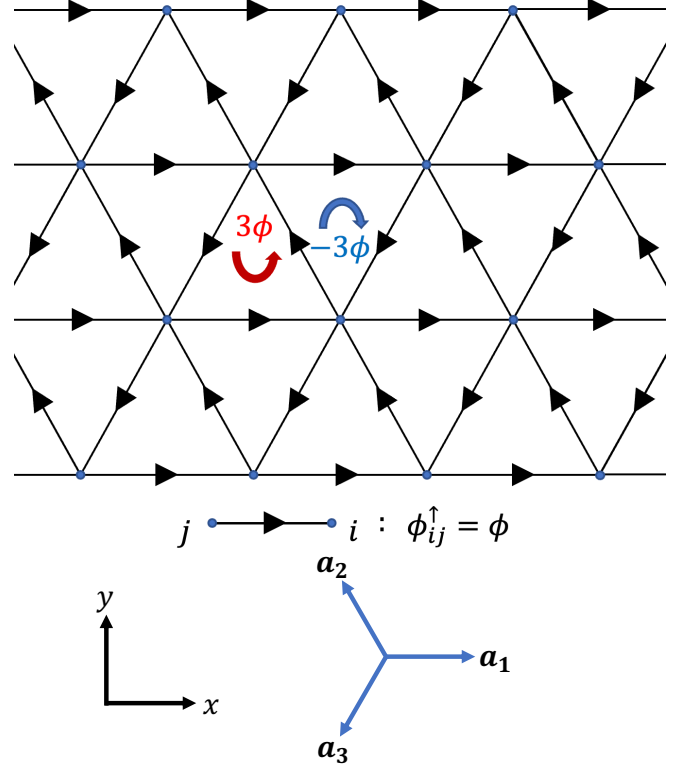


FIG. 1. (color online). Illustration of the flux pattern for the valley \uparrow . The other valley is related by time reversal symmetry and has opposite flux pattern.

Hamiltonian to perform the calculation:

$$\begin{aligned}
 H_{\text{MF}} = & - \sum_{\langle ij \rangle, s} (t e^{i\phi_{ij}^s} \langle b_i b_j^\dagger \rangle f_{i,s}^\dagger f_{j,s} + \text{H.c.}) \\
 & - \frac{J}{8} \sum_{\langle ij \rangle, s} \left[\left(\chi_{ij,s}^* + 2e^{i2\phi_{ij}^s} \chi_{ij,-s}^* \right) f_{i,s}^\dagger f_{j,s} + \text{H.c.} \right] \\
 & + \frac{J}{8} \sum_{\langle ij \rangle} \left[\left(\Delta_{ij} + 2\Delta_{ji} e^{i2\phi_{ij}^\uparrow} \right) f_{i,\uparrow}^\dagger f_{j,\downarrow}^\dagger + (i \leftrightarrow j) + \text{H.c.} \right] \\
 & - \mu \sum_i (n_{i\uparrow} + n_{i\downarrow}),
 \end{aligned} \tag{3}$$

with $\chi_{ij,s} = 2 \langle f_{i,s}^\dagger f_{j,s} \rangle$ and $\Delta_{ij} = 2 \langle f_{i\uparrow}^\dagger f_{j\downarrow} \rangle$. The chemical potential μ is tuned to make $\frac{1}{N} \sum_{i,s} \langle n_{i,s} \rangle = 1 - x$, where x is the doping level. We ignore the magnetic order since it is suppressed on doping level greater than a critical value x_c [32]. Moreover, we assume that the system respects the translation symmetry, then the bosons are condensed and satisfying $\langle b_i b_j^\dagger \rangle = \langle b_j^\dagger b_i \rangle = x$ [32]. We can simply take $\langle b \rangle = \sqrt{x}$.

As for $n > 1$ case, we can apply a particle hole transformation $c_{i,s} \rightarrow c_{i,-s}^\dagger$ on the original Hamiltonian and apply the same procedure. By solving the self-consistent equation, we obtained the order parameter dependence on ϕ and n . The result is shown in Fig.2.

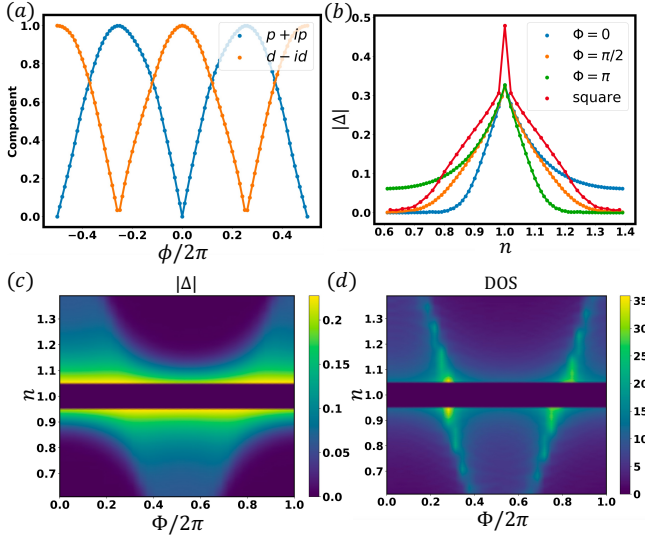


FIG. 2. (color online). $t/J = 3$. (a) Dependence of $p+ip$ and $d-id$ pairing's component on ϕ at $n = 0.9$. (b) Dependence of $|\Delta| = |\Delta_{ij}|$ on the density n while flux $\Phi = 0, \pi/2$ on triangular lattice and $\Phi = 0$ on square lattice. (c) Dependence of $|\Delta|$ on Φ and n . (d) Dependence of DOS on Φ and n . In (c) and (d), the region $0.95 < n < 1.05$ is removed because the superconductivity is expected to be suppressed because the slave boson condensation $\langle b \rangle = \sqrt{x}$ is weak in this regime.

P wave vs d wave– The special case with $\Phi = 0$ has been studied before [32]. There $\Delta_{ij} = \Delta e^{\pm i2\theta_{ij}}$ is in the $d_{x^2-y^2} \pm id_{xy}$ pairing symmetry. With a finite Φ , the spin rotation symmetry is broken down to $U(1)$ generated by the S_z rotation. Therefore, the relation $\Delta_{ij} = \Delta_{ji}$ would not hold anymore and generically the pairing symmetry is a superposition of spin-triplet p wave and spin-singlet d wave. Δ_{ij} and Δ_{ji} have the same magnitude but different phases. Since Δ_{ij} respects C_3 symmetry instead of C_6 symmetry, the angular momentum is defined mod 3. The $p \pm ip$ and $d \mp id$ pairings are mixed, we can define their components as $\Delta_p = \frac{1}{2|\Delta_{ij}|}|\Delta_{ij} - \Delta_{ji}|$ and $\Delta_d = \frac{1}{2|\Delta_{ij}|}|\Delta_{ij} + \Delta_{ji}|$. The components' dependence on ϕ is shown in Fig.2(a).

We note that the superconducting order breaks the time reversal symmetry \mathcal{T} and mirror reflection symmetry $\mathcal{M}_x(\mathcal{M}_y)$, but satisfied the combined mirror time reversal $\mathcal{M}_x\mathcal{T}(\mathcal{M}_y\mathcal{T})$ symmetry combined with a $U(1)$ transformation.

Pairing strength– We study the dependence of $|\Delta_{ij}|$ on different value of n and Φ . As shown in Fig.2(b)(c), the superconducting gap $|\Delta|$ is larger at electron doping than hole doping when $0 \leq \Phi < \frac{\pi}{2}$ and $\frac{3\pi}{2} < \Phi \leq 2\pi$, and smaller when $\frac{\pi}{2} < \Phi < \frac{3\pi}{2}$. The reason is that the DOS of the free dispersion does not respect particle hole symmetry, and the Van Hove peak locates at $n > 1$ for the former case, $n < 1$ for the latter case. The apparent correlation between the pairing strength and the DOS in Fig. 3(d) suggest that we should look for superconductor

close to the Van Hove singularity, which is tunable by gating in the twisted TMD homo-bilayer.

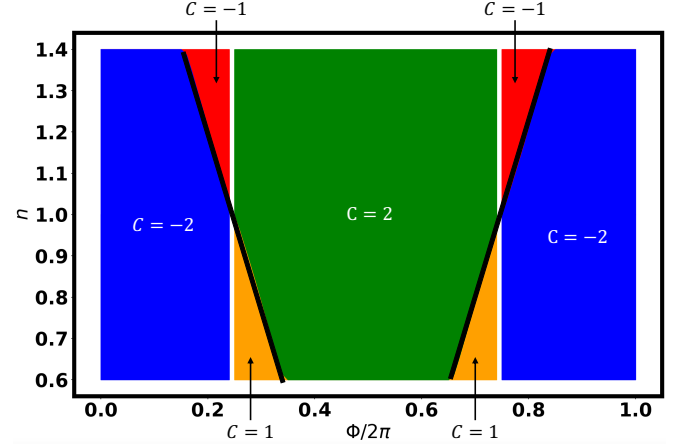


FIG. 3. (color online). $t/J = 3$. Dependence of Chern number on n and Φ for fixed chirality. The black and white line corresponds to one and three Dirac nodes in the dispersion plot.

Topological property– The chiral superconductor is known to host a non-zero Chern number, which could be calculated via [42]:

$$C = \frac{1}{4\pi} \int_{\text{BZ}} d^2\mathbf{k} [\hat{\mathbf{m}} \cdot (\partial_{k_x} \hat{\mathbf{m}} \times \partial_{k_y} \hat{\mathbf{m}})], \quad (4)$$

where $\hat{\mathbf{m}} = \frac{1}{\sqrt{\epsilon_k^2 + |\Delta_k|^2}}(\text{Re}\Delta_k, \text{Im}\Delta_k, \epsilon_k)$. The definition is equivalent to the winding number of Δ_k as k moves around the Fermi surface in the anti-clockwise direction. We can also calculate the winding number by counting the number of Δ 's zero points inside the Fermi sphere, the formula is $C = \#_1 - \#_2$, where $\#_1$ and $\#_2$ represent the number of saddles and sources respectively. The phase diagram is shown in Fig.3 provided that the chirality is fixed. The change in Chern number equals to the number of Dirac nodes at the transition point. There are two kinds of transitions, which corresponds to one Dirac node (at κ point) and three Dirac nodes (inside the mini Brillouin zone) closing the gap respectively. For details, please see Appendix.A.

Effects of ϕ – The phase of hopping parameters ϕ_{ij}^s plays two roles in our model: (1) It can produce an effective magnetic flux in the t term. (2) It enters the spin-spin coupling J term. The first one changes the distribution of DOS and the second one changes the form of pairing. To study these two effects in detail, we change the kinetic term and the interaction term in Eq.2 to the conventional t-J model's form, which are named \tilde{t} -J model and \tilde{t} - \tilde{J} model respectively. We note that ϕ and $\phi + \frac{2\pi}{3}$ could no more be related via a gauge transformation here. In \tilde{t} - \tilde{J} model, we find that the superconducting order parameter returns to nearly pure d wave pairing shown in Fig.4(a), but the hopping term still acquires a phase based on the mean field calculation. As shown in

Fig.4(b), the components' dependence on ϕ in \tilde{t} -J model is nearly the same as the original model. Therefore, we can conclude that the pairing symmetry is decided by the J term as expected. In \tilde{t} -J model, the phase of the hopping parameter is found to be relatively small, especially at high doping levels. It makes the effective flux become smaller than the original Hamiltonian, causing the superconducting gap to become less dependent on ϕ as shown in Fig.4(c)-(d).

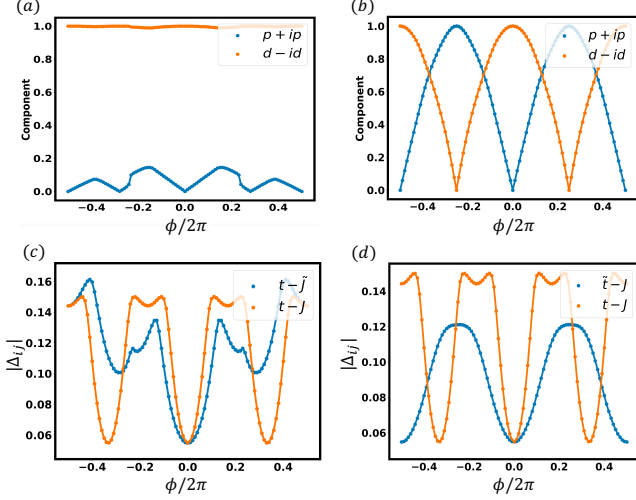


FIG. 4. (color online). $t/J = 3$. (a)-(b) Components of $p+ip$ and $d-id$ at $n = 0.9$ for t -J model and \tilde{t} -J model respectively. (c)-(d) The superconducting gap $|\Delta_{ij}|$ at $n = 0.88$ for t -J model and \tilde{t} -J model respectively.

Nematic nodal superconductor from strain—So far we have only observed gapped chiral superconductor respecting C_3 symmetry. One may expect that a nematic superconductor with mixing between $l = 1$ and $l = -1$ angular momentum channels is a competing state. In the following we show that a small strain can easily favor a nematic nodal superconductor. We consider the effects of strain by multiplying a factor $(1 - \alpha)$ on the hopping parameter $te^{i\phi_{ij}^s}$ on the bond along the x -axis, i.e., $t_{i\pm\mathbf{a}_1,i}$, where α implies the stress intensity. Since $J_{ij} = \frac{t_{ij}^2}{U}$, the J term needs to be multiplied by a factor $(1 - \alpha)^2$ along the x -axis. When $\alpha = 1$, the Hamiltonian is reduced to the one on the square lattice, where the pairing symmetry is known to be $d_{x^2-y^2}$. Therefore, the time reversal symmetry and mirror reflection symmetry can be restored by sufficiently large strain. During the calculation, the pairing parameter $\Delta_{i\pm\mathbf{a}_1,i}$ is found to decay very fast when α grows. It shows that the $d_{x^2-y^2}$ superconductor in the square lattice can be reached by small α . We use $1 - \langle \mathcal{T} \rangle$ and $1 - \langle \mathcal{M}_y \rangle$ to label the symmetry of the ground states. Here $\langle \mathcal{T} \rangle$ is defined by the inner product of the ground states of H and $\mathcal{T}H\mathcal{T}^{-1}$, and similar for \mathcal{M}_y . Since the Hamiltonian has a global U(1) symmetry, $\langle \mathcal{T} \rangle$ and $\langle \mathcal{M}_y \rangle$ will change as the global phase θ changes. Therefore, we need to choose the appropriate θ to maximize the ex-

pected value to represent the symmetry faithfully. As shown in Fig.6, the time reversal symmetry and mirror reflection symmetry can be restored by a small strain. In Fig.6(d), we show that there are four nodes in the resulting superconductor phase under strain. This calculation demonstrates that a nodal nematic superconductor is indeed a strong competing state and can be favored by a small strain. It is interesting to also study the possibility that the C_3 symmetry is spontaneously broken by additional terms.

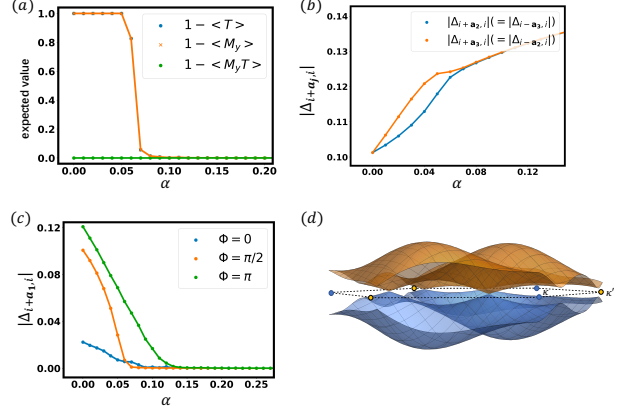


FIG. 5. (color online). $t/J = 3$, $n = 0.85$. (a) The expected value of time reversal operator, mirror reflection operator and mirror time reversal operator as α changes for flux $\Phi = \frac{\pi}{2}$. (b) Dependence of $|\Delta_{i+\mathbf{a}_2,i}| (= |\Delta_{i-\mathbf{a}_3,i}|)$ and $|\Delta_{i+\mathbf{a}_3,i}| (= |\Delta_{i-\mathbf{a}_2,i}|)$ on α for $\Phi = \frac{\pi}{2}$ with the chirality fixed. (c) Dependence of $|\Delta_{i+\mathbf{a}_1,i}|$ on α for flux $\Phi = 0, \frac{\pi}{2}, \pi$. (d) The dispersion plot for $\Phi = \frac{\pi}{2}$, $\alpha = 0.15$, the gap closes at 4 nodal points in the first Brillouin zone.

The effect of three-site hopping term—In addition to Eq.2, perturbation theory also gives a three-site hopping term [43], it can be written as:

$$H_{t_3} = -t_3 \sum_{\langle ijk \rangle, s} P \left(n_{j,-s} c_{k,s}^\dagger c_{i,s} e^{i2\phi_{kj}^s} - c_{k,s}^\dagger c_{j,-s}^\dagger c_{j,s} c_{i,-s} + \text{H.c.} \right) P, \quad (5)$$

where $t_3 = \frac{J}{4}$. Here we suppose t_3 can be changed independently in order to discuss this term's effect. By applying the slave boson approach mentioned above, we can read off this term as:

$$H_{t_3} = -t_3 \sum_{\langle ijk \rangle, s} \left(b_k b_i^\dagger f_{j,-s}^\dagger f_{j,-s} f_{k,s}^\dagger f_{i,s} e^{i2\phi_{kj}^s} - b_k b_i^\dagger f_{k,s}^\dagger f_{j,-s}^\dagger f_{j,-s} f_{i,-s} + \text{H.c.} \right), \quad (6)$$

where $b_k b_i^\dagger \approx \langle b_k b_i^\dagger \rangle = x$ is the doping level, so this term's effect increases as the doping level increases. Indeed, Eq.6 can be decoupled in the pairing channel [43] as:

$$H_{t_3} = xt_3 \sum_{\langle ij \rangle} \left[\Delta_{ij} (\Delta_{ji}^* e^{i2\phi_{ji}^\dagger} + \Delta_{ij}^*) + \text{H.c.} \right] \quad (7)$$

So we can expect that a positive value of t_3 can increase the total energy, leading to a decrease in $|\Delta_{ij}|$ by solving the self-consistent equation. The mean field calculation validates our expectation as shown in Fig.6(a). This suggests that the $n > 1$ side would have stronger superconductor than the $n < 1$ side even for the particle-hole symmetric point $\Phi = \frac{\pi}{2}$.

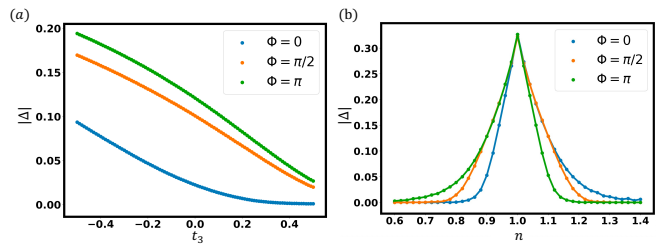


FIG. 6. (color online). $t/J = 3$. (a) Dependence of $|\Delta|$ on t_3 for $n = 0.85$. (b) Dependence of $|\Delta|$ on n for $t_3 = 0.25J$.

Summary– In conclusion, we use a slave boson method to investigate a t-J model with valley contrasting flux in the context of twisted TMD homobilayer. We show that the superconducting order parameter is a mixture of $p-ip$ and $d+id$ pairing when $\phi \neq 0$. We notice two topological phase transitions with jump of Chern numbers by tuning the valley contrasting flux Φ , which is controlled by the vertical displacement field in the TMD homo-bilayer. The pairing strength correlates with the density of states (DoS), suggesting that we should search for superconductor near the van Hove singularity. Finally, we find that a small strain can favor a nematic nodal superconductor similar to the $d_{x^2-y^2}$ pairing on the square lattice.

Acknowledgement This work is supported by a startup fund from the Johns Hopkins University.

-
- [1] P. A. Lee, N. Nagaosa, and X.-G. Wen, Doping a mott insulator: Physics of high-temperature superconductivity, *Rev. Mod. Phys.* **78**, 17 (2006).
 - [2] Y. Cao, V. Fatemi, A. Demir, S. Fang, S. L. Tomarken, J. Y. Luo, J. D. Sanchez-Yamagishi, K. Watanabe, T. Taniguchi, E. Kaxiras, *et al.*, Correlated insulator behaviour at half-filling in magic-angle graphene superlattices, *Nature* **556**, 80 (2018).
 - [3] G. Chen, A. L. Sharpe, P. Gallagher, I. T. Rosen, E. Fox, L. Jiang, B. Lyu, H. Li, K. Watanabe, T. Taniguchi, *et al.*, Signatures of gate-tunable superconductivity in trilayer graphene/boron nitride moiré superlattice, *arXiv e-prints*, arXiv (2019).
 - [4] G. Chen, L. Jiang, S. Wu, B. Lyu, H. Li, B. L. Chittari, K. Watanabe, T. Taniguchi, Z. Shi, J. Jung, *et al.*, Evidence of a gate-tunable mott insulator in a trilayer graphene moiré superlattice, *Nature Physics* **15**, 237 (2019).
 - [5] M. Yankowitz, S. Chen, H. Polshyn, Y. Zhang, K. Watanabe, T. Taniguchi, D. Graf, A. F. Young, and C. R. Dean, Tuning superconductivity in twisted bilayer graphene, *Science* **363**, 1059 (2019).
 - [6] G. Chen, A. L. Sharpe, E. J. Fox, Y.-H. Zhang, S. Wang, L. Jiang, B. Lyu, H. Li, K. Watanabe, T. Taniguchi, *et al.*, Tunable correlated chern insulator and ferromagnetism in a moiré superlattice, *Nature* **579**, 56 (2020).
 - [7] X. Lu, P. Stepanov, W. Yang, M. Xie, M. A. Aamir, I. Das, C. Urgell, K. Watanabe, T. Taniguchi, G. Zhang, *et al.*, Superconductors, orbital magnets and correlated states in magic-angle bilayer graphene, *Nature* **574**, 653 (2019).
 - [8] Y. Cao, D. Rodan-Legrain, O. Rubies-Bigorda, J. M. Park, K. Watanabe, T. Taniguchi, and P. Jarillo-Herrero, Tunable correlated states and spin-polarized phases in twisted bilayer-bilayer graphene, *Nature* **583**, 215 (2020).
 - [9] X. Liu, Z. Hao, E. Khalaf, J. Y. Lee, Y. Ronen, H. Yoo, D. H. Najafabadi, K. Watanabe, T. Taniguchi, A. Vishwanath, *et al.*, Tunable spin-polarized correlated states in twisted double bilayer graphene, *Nature* **583**, 221 (2020).
 - [10] C. Shen, Y. Chu, Q. Wu, N. Li, S. Wang, Y. Zhao, J. Tang, J. Liu, J. Tian, K. Watanabe, *et al.*, Correlated states in twisted double bilayer graphene, *Nature Physics*, 1 (2020).
 - [11] H. Polshyn, J. Zhu, M. A. Kumar, Y. Zhang, F. Yang, C. L. Tschirhart, M. Serlin, K. Watanabe, T. Taniguchi, A. H. MacDonald, *et al.*, Electrical switching of magnetic order in an orbital chern insulator, *Nature* **588**, 66 (2020).
 - [12] S. Chen, M. He, Y.-H. Zhang, V. Hsieh, Z. Fei, K. Watanabe, T. Taniguchi, D. H. Cobden, X. Xu, C. R. Dean, *et al.*, Electrically tunable correlated and topological states in twisted monolayer-bilayer graphene, *Nature Physics* **17**, 374 (2021).
 - [13] A. L. Sharpe, E. J. Fox, A. W. Barnard, J. Finney, K. Watanabe, T. Taniguchi, M. Kastner, and D. Goldhaber-Gordon, Emergent ferromagnetism near three-quarters filling in twisted bilayer graphene, *Science* **365**, 605 (2019).
 - [14] M. Serlin, C. Tschirhart, H. Polshyn, Y. Zhang, J. Zhu,

- K. Watanabe, T. Taniguchi, L. Balents, and A. Young, Intrinsic quantized anomalous hall effect in a moiré heterostructure, *Science* **367**, 900 (2020).
- [15] Y. Tang, L. Li, T. Li, Y. Xu, S. Liu, K. Barmak, K. Watanabe, T. Taniguchi, A. H. MacDonald, J. Shan, *et al.*, Simulation of hubbard model physics in wse 2/wse 2 moiré superlattices, *Nature* **579**, 353 (2020).
- [16] E. C. Regan, D. Wang, C. Jin, M. I. B. Utama, B. Gao, X. Wei, S. Zhao, W. Zhao, Z. Zhang, K. Yumigeta, *et al.*, Mott and generalized wigner crystal states in wse 2/wse 2 moiré superlattices, *Nature* **579**, 359 (2020).
- [17] L. Wang, E.-M. Shih, A. Ghiotto, L. Xian, D. A. Rhodes, C. Tan, M. Claassen, D. M. Kennes, Y. Bai, B. Kim, *et al.*, Correlated electronic phases in twisted bilayer transition metal dichalcogenides, *Nature materials* **19**, 861 (2020).
- [18] J. Gu, L. Ma, S. Liu, K. Watanabe, T. Taniguchi, J. C. Hone, J. Shan, and K. F. Mak, Dipolar excitonic insulator in a moiré lattice, *Nature Physics* **18**, 395 (2022).
- [19] Z. Zhang, E. C. Regan, D. Wang, W. Zhao, S. Wang, M. Sayyad, K. Yumigeta, K. Watanabe, T. Taniguchi, S. Tongay, *et al.*, Correlated interlayer exciton insulator in double layers of monolayer wse2 and moiré wse2/wse2, arXiv preprint arXiv:2108.07131 (2021).
- [20] T. Li, S. Jiang, L. Li, Y. Zhang, K. Kang, J. Zhu, K. Watanabe, T. Taniguchi, D. Chowdhury, L. Fu, *et al.*, Continuous mott transition in semiconductor moiré superlattices, *Nature* **597**, 350 (2021).
- [21] A. Ghiotto, E.-M. Shih, G. S. Pereira, D. A. Rhodes, B. Kim, J. Zang, A. J. Millis, K. Watanabe, T. Taniguchi, J. C. Hone, *et al.*, Quantum criticality in twisted transition metal dichalcogenides, *Nature* **597**, 345 (2021).
- [22] T. Li, S. Jiang, B. Shen, Y. Zhang, L. Li, Z. Tao, T. Devakul, K. Watanabe, T. Taniguchi, L. Fu, *et al.*, Quantum anomalous hall effect from intertwined moiré bands, *Nature* **600**, 641 (2021).
- [23] Y. Cao, V. Fatemi, S. Fang, K. Watanabe, T. Taniguchi, E. Kaxiras, and P. Jarillo-Herrero, Unconventional superconductivity in magic-angle graphene superlattices, *Nature* **556**, 43 (2018).
- [24] J. M. Park, Y. Cao, K. Watanabe, T. Taniguchi, and P. Jarillo-Herrero, Tunable strongly coupled superconductivity in magic-angle twisted trilayer graphene, *Nature* **590**, 249 (2021).
- [25] Z. Hao, A. Zimmerman, P. Ledwith, E. Khalaf, D. H. Najafabadi, K. Watanabe, T. Taniguchi, A. Vishwanath, and P. Kim, Electric field-tunable superconductivity in alternating-twist magic-angle trilayer graphene, *Science* **371**, 1133 (2021).
- [26] H. C. Po, L. Zou, A. Vishwanath, and T. Senthil, Origin of mott insulating behavior and superconductivity in twisted bilayer graphene, *Physical Review X* **8**, 031089 (2018).
- [27] F. Wu, T. Lovorn, E. Tutuc, and A. H. MacDonald, Hubbard model physics in transition metal dichalcogenide moiré bands, *Physical review letters* **121**, 026402 (2018).
- [28] Here we focus on the AA stacking. The case of AB stacking is very different[44].
- [29] H. Pan, F. Wu, and S. D. Sarma, Band topology, hubbard model, heisenberg model, and dzyaloshinskii-moriya interaction in twisted bilayer wse 2, *Physical Review Research* **2**, 033087 (2020).
- [30] J. Wang, J. Zang, J. Cano, and A. J. Millis, Staggered pseudo magnetic field in twisted transition metal dichalcogenides: Physical origin and experimental consequences, arXiv preprint arXiv:2110.14570 (2021).
- [31] Y.-H. Zhang and T. Senthil, Bridging hubbard model physics and quantum hall physics in trilayer graphene/h-bn moiré superlattice, *Physical Review B* **99**, 205150 (2019).
- [32] Q.-H. Wang, D.-H. Lee, and P. A. Lee, Doped $t-j$ model on a triangular lattice: Possible application to $\text{Na}_x\text{CoO}_2 \cdot y\text{H}_2\text{O}$ and $\text{Na}_{1-x}\text{TiO}_2$, *Phys. Rev. B* **69**, 092504 (2004).
- [33] Y.-M. Wu, Z. Wu, and H. Yao, Pair-density-wave and chiral superconductivity in twisted bilayer transition-metal-dichalcogenides, arXiv preprint arXiv:2203.05480 (2022).
- [34] Z. Wu, Y.-M. Wu, and F. Wu, Pair density wave and loop current promoted by van hove singularities in moiré systems, arXiv preprint arXiv:2207.11468 (2022).
- [35] A. Wietek, J. Wang, J. Zang, J. Cano, A. Georges, and A. Millis, Tunable stripe order and weak superconductivity in the moiré hubbard model, arXiv preprint arXiv:2204.04229 (2022).
- [36] Y.-F. Jiang and H.-C. Jiang, Topological superconductivity in the doped chiral spin liquid on the triangular lattice, *Physical Review Letters* **125**, 157002 (2020).
- [37] Y. Huang, S.-S. Gong, and D. Sheng, Emergent topological chiral superconductivity in a triangular-lattice $t-j$ model, arXiv preprint arXiv:2209.00833 (2022).
- [38] Y. Huang and D. Sheng, Topological chiral and nematic superconductivity by doping mott insulators on triangular lattice, *Physical Review X* **12**, 031009 (2022).
- [39] H. Pan, F. Wu, and S. Das Sarma, Band topology, hubbard model, heisenberg model, and dzyaloshinskii-moriya interaction in twisted bilayer wse₂, *Phys. Rev. Research* **2**, 033087 (2020).
- [40] I. Hubač and S. Wilson, Brillouin-wigner methods for many-body systems, in *Brillouin-Wigner Methods for Many-Body Systems* (Springer, 2010) pp. 133–189.
- [41] J. Brinckmann and P. A. Lee, Renormalized mean-field theory of neutron scattering in cuprate superconductors, *Phys. Rev. B* **65**, 014502 (2001).
- [42] N. Read and D. Green, Paired states of fermions in two dimensions with breaking of parity and time-reversal symmetries and the fractional quantum hall effect, *Phys. Rev. B* **61**, 10267 (2000).
- [43] B. Ammon, M. Troyer, and H. Tsunetsugu, Effect of the three-site hopping term on the $t-j$ model, *Phys. Rev. B* **52**, 629 (1995).
- [44] Y.-H. Zhang, D. Sheng, and A. Vishwanath, Su (4) chiral spin liquid, exciton supersolid, and electric detection in moiré bilayers, *Physical review letters* **127**, 247701 (2021).

Appendix A: Topological transitions

In the main text, we observe that Chern number depends on Φ and n . There are two kinds of topological transitions, which corresponds to one Dirac node and three Dirac nodes respectively. The sketch of the dispersion plot for two

different situations is shown in Fig.7.

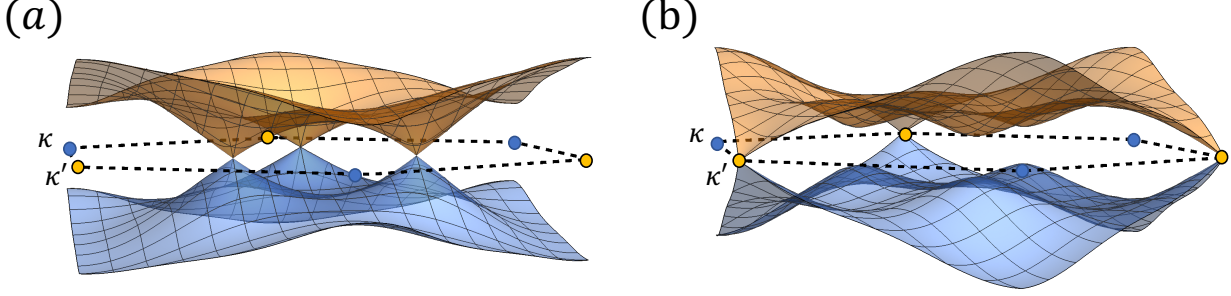


FIG. 7. (color online). (a) Illustration of the three Dirac nodes inside the first Brillouin zone. (b) Illustration of the Dirac node at κ' .

Appendix B: Stability of the Dirac nodes

In the main text, we show that the Chern number has two kinds of transitions while varying the parameters. Here we demonstrate that the transitions will remain the same type under perturbations respecting C_3 symmetry. This fact can be verified by calculating the number of the Dirac nodes at the transition point. The Dirac node corresponds to the point in the first Brillouin zone where $\Delta(\mathbf{k})$ and $\epsilon(\mathbf{k})$ vanish simultaneously. In our system, the C_3 symmetry in the Hamiltonian requires that $\Delta(C_3\mathbf{k}) = \Delta(\mathbf{k})$ and $\epsilon(C_3\mathbf{k}) = \epsilon(\mathbf{k})$. Therefore, the Dirac node in the transition points that the Chern number only change by 1 locates at Γ , κ or κ' . The superconducting order parameter in k -space can be written as:

$$\Delta(\mathbf{k}) = 2|\Delta| \sum_{j=1,2,3} e^{i\frac{2\pi}{3}(j-1)} \cos(\mathbf{k} \cdot \mathbf{a}_j - \phi_{\text{SC}}), \quad (\text{B1})$$

here ϕ_{SC} is defined by the relation $\Delta_{i+\mathbf{a}_j,i} = e^{-i2\phi_{\text{SC}}} \Delta_{i-\mathbf{a}_j,i}$. The expression around Γ , κ or κ' can be expanded as:

$$\Delta(\mathbf{k}) = 3|\Delta|\beta(k_x + ik_y), \quad (\text{B2})$$

where $\beta = \sin\phi_{\text{SC}}, \sin(\phi_{\text{SC}} + \frac{2\pi}{3}), \sin(\phi_{\text{SC}} - \frac{2\pi}{3})$ corresponds to Γ , κ , κ' respectively. Any rotation around z -axis is equivalent to a $U(1)$ gauge transform. The solutions of $\Delta(\mathbf{k}) = 0$ can only be shifted by adding a constant, which breaks the z -rotation symmetry. Therefore, we can conclude that the existence of the Dirac node at Γ , κ or κ' is robust under perturbations respecting C_3 symmetry. This can be illustrated by considering the three-site term 6 and next-nearest-neighbor (NNN) hopping:

$$H_{t_2} = -t_2 \sum_{\langle\langle ij \rangle\rangle, s} P(c_{i,s}^\dagger c_{j,s} + \text{H.c.})P, \quad (\text{B3})$$

where $\langle\langle ij \rangle\rangle$ represents NNN sites. As shown in Fig.8, the transition of the Chern number remains the same pattern.

Appendix C: Symmetry transformation on the order parameters

We note that the order parameters in Eq.3 has 12 degrees of freedom, in which 6 corresponds to the pairing in six bonds, they are $\Delta_{i\pm\mathbf{a}_j,i}$, $j = 1, 2, 3$, where $\mathbf{a}_1 = (1, 0)$, $\mathbf{a}_2 = (-\frac{1}{2}, \frac{\sqrt{3}}{2})$, $\mathbf{a}_3 = (-\frac{1}{2}, -\frac{\sqrt{3}}{2})$ and $\mathbf{a}_{j+3} = \mathbf{a}_j$. The remaining $6 = 3 + 3$ corresponds to the hopping parameters in spin up and down channels, they are $\chi_{i+\mathbf{a}_j,i,\uparrow}$ and $\chi_{i+\mathbf{a}_j,i,\downarrow}$, $j = 1, 2, 3$. Under C_6 rotation, the order parameters transform as $\Delta_{i+\mathbf{a}_j,i} \rightarrow -\Delta_{i+\mathbf{a}_{j-1},i}$, $\chi_{i+\mathbf{a}_j,i,s} \rightarrow \chi_{i-\mathbf{a}_{j-1},i,-s}$. Under time reversal transformation, the order parameters transform as $\Delta_{i\pm\mathbf{a}_j,i} \rightarrow -\Delta_{i\mp\mathbf{a}_j,i}^*$ and $\chi_{i\pm\mathbf{a}_j,i,s} \rightarrow \chi_{i\pm\mathbf{a}_j,i,-s}^*$. Under mirror reflection transformation about the x -axis, the order parameters transform as $\Delta_{i\pm\mathbf{a}_j,i} \rightarrow \Delta_{i\pm\mathbf{a}_{5-j},i}$ and $\chi_{i\pm\mathbf{a}_j,i,s} \rightarrow \chi_{i\pm\mathbf{a}_{5-j},i,s}$. Under mirror reflection transformation about the y -axis, the order parameters transform as $\Delta_{i\pm\mathbf{a}_j,i} \rightarrow -\Delta_{i\pm\mathbf{a}_{5-j},i}$ and $\chi_{i\pm\mathbf{a}_j,i,s} \rightarrow \chi_{i\mp\mathbf{a}_{5-j},i,-s}$.

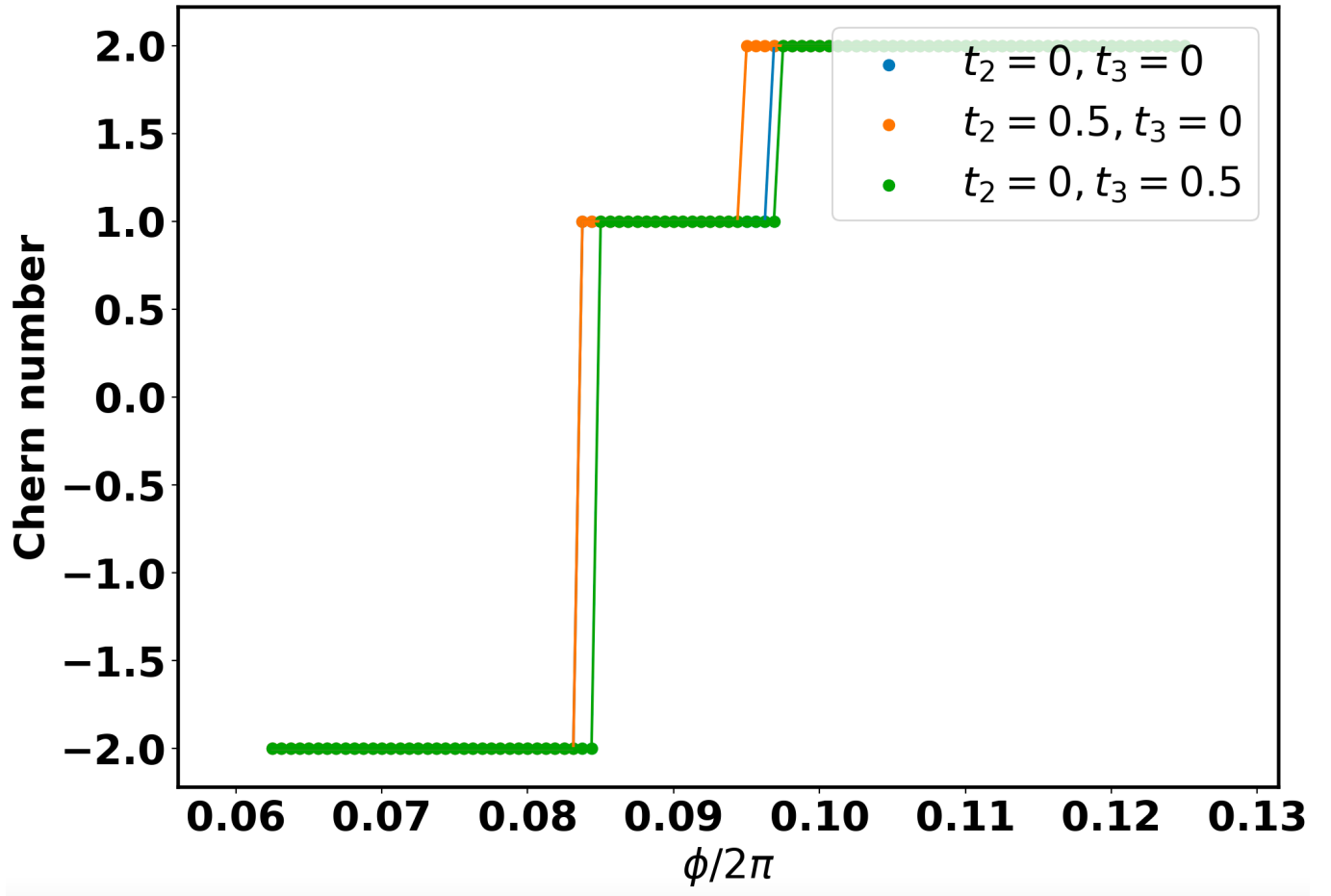


FIG. 8. (color online). Dependence of the Chern number on ϕ at $n = 0.85$.

From the above analysis, one can verify that under mirror time reversal transformation about the x -axis, the order parameters transform as $\Delta_{i\pm\mathbf{a}_j,i} \rightarrow -\Delta_{i\mp\mathbf{a}_5-j,i}^*$ and $\chi_{i\pm\mathbf{a}_j,i,s} \rightarrow \chi_{i\pm\mathbf{a}_5-j,i,-s}^*$. Under mirror time reversal transformation about the y -axis, the order parameters transform as $\Delta_{i\pm\mathbf{a}_j,i} \rightarrow \Delta_{i\mp\mathbf{a}_5-j,i}^*$ and $\chi_{i\pm\mathbf{a}_j,i,s} \rightarrow \chi_{i\mp\mathbf{a}_5-j,i,s}^*$. The mean field results give that the order parameters are gauge equivalent to the ones before the symmetry transformation.